Crystallographic Texture and Orientation Variants in Al_2O_3-$Y_3Al_5O_{12}$ Directionally Solidified Eutectic Crystals

Colleen S. Frazer[a], Elizabeth C. Dickey[a,*] and Ali Sayir[b,§]

[a] Department of Chemical and Materials Engineering, University of Kentucky, Lexington, KY

[b] NASA Glenn Research Center, Cleveland, OH

Abstract

Eutectic rods of Al_2O_3 and $Y_3Al_5O_{12}$ were grown by a laser-heated float zone method, and their microstructure and crystallographic texture were studied by scanning electron microscopy, electron backscattered diffraction and x-ray diffraction. The composites were found to be highly textured with two twin-related crystallographic orientation relationships between the phases. Electron backscattered diffraction was employed to determine the spatial distribution of the orientational variants within the samples and to define the crystallographic orientation of various microstructural features.

PACS: 61.10.Nz; 61.16.Yc; 61.72.Mm; 68.35.Ct; 81.05.M; 81.10.Fq

Key Words: A1.Characterization, A1.Directional Solidification, A1.Eutectics, A1.Interfaces, A2.Floating Zone Technique, B1.Oxides

* Please direct correspondence to: A254 ASTeCC Build., Lexington, KY 40506-0286; tel: (859)257-2300 x288; FAX: (859) 257-2489; ecdickey@engr.uky.edu

§ Case Western Reserve University

1. Introduction

Oxide directionally solidified eutectics (DSEs) have received considerable attention over the past twenty years because of their unique, highly anisotropic mechanical, optical and transport properties [1-4]. Because the system is at a eutectic composition, the material solidifies as an *in-situ* composite with an organized microstructure, ranging from fibrous to lamellar depending primarily upon the volume fractions of the constituent phases [5,6]. Furthermore, the directional solidification process usually results in highly textured materials with well-defined crystallographic orientation relationships between the two phases [1,2,7]. The Al_2O_3-$Y_3Al_5O_{12}$ (YAG) DSE, in particular, has attracted much interest for its potential use as an ultra-high-temperature structural material because of its oxidation resistance, microstructural stability and excellent high-temperature strength and creep resistance [8-12]. It has been shown, in fact, that the compressive creep stress of YAG-Al_2O_3 DSEs is approximately 13 times higher than isotropic sintered samples having the same chemical composition [13]. The mechanical properties of DSEs are, however, very sensitive to microstructure and crystallographic texture, which can vary with processing conditions [14,15]. Consequently, it is important to be able to fully quantify the microstructure and crystallographic texture of these materials in order to predict material performance.

This paper provides a detailed analysis of Al_2O_3-YAG DSE filaments grown by the laser-heated float zone method. While pole figure analysis by x-ray diffraction is a standard and useful technique for measuring crystallographic texture, it only provides information averaged over the diffracting volume, typically on the order of at least 100 μm in the lateral and depth directions. Often, as will become apparent below, it is insightful to have spatially resolved information about the crystallographic orientations of the constituent phases. Electron

backscattered diffraction (EBSD) performed in a scanning electron microscope (SEM) provides such detailed, spatially-resolved orientation information by giving phase-specific crystallographic data from volumes on the order of one micron. Moreover, the crystallography can be mapped over large areas of the specimen by orientation imaging microscopy (OIM). OIM facilitates correlation of microstructure and crystallography, yielding additional information about the distribution of orientational variants and the crystallographic orientation of various microstructural features. In this paper we demonstrate the utility of these techniques for quantifying and correlating microstructure and crystallography in directionally solidified Al_2O_3-YAG eutectics.

2. Experimental procedures

2.1 Crystal growth

Al_2O_3-YAG directionally solidified eutectics were grown using the laser-heated float zone method (LHFZ). The growth process differed from conventional laser-heated float zone in two aspects: source rod preparation and heating configuration. For preparation of the source rod, high purity (99.999% pure) polycrystalline alumina powder was obtained from CERAC/pure[†] (325 mesh) and 99.999 % pure Y_2O_3 from Alpha Products. The powders were blended with 5% wt.% Methocel 20-231® plus glycerin in a water-based slurry. The slurry was degassed overnight under a moderate vacuum (~$70x10^3$ Pa) to achieve a high viscosity paste. The paste was subsequently extruded with a custom-made mini-extruder, fabricated with plastic components in high-wear regions to prevent contamination of the slurry. At least two extrusions

[†] Ceralox Corp., Tucson, AZ 08576.
® The Dow Chemical Company, Midland, MI 48674.

were made to minimize porosity in the paste. The extruded source rod was normally 2 to 5 mm in diameter and extruded lengths were 15 to 20 cm long. The rods were furnace dried in air at 200 °C for approximately 1 hour and were placed in the LHFZ apparatus without any pre-sintering.

The LHFZ apparatus was designed to be a fully automatic, computer-controlled rod processing facility. A coherent CO_2-laser beam (FH-1500-Carbon Dioxide Laser)[#] was used for the heating source. The laser was split into four orthogonal beams, which were focused with zinc-selenide lenses onto the molten zone at the top of a polycrystalline alumina/yittria source rod in the center of the processing chamber. These opposing beams were converted into laser line scans that provided uniform heating at the circumference of the molten zone.

For single-crystal rod growth, a seed crystal (single-crystal sapphire of c-axis orientation) was lowered onto the molten liquid until wetting occurred. The source rod was moved vertically, via computer control, through the laser beam at a constant velocity. The maximum available laser power was 800 watts, but only 30-40% of this power was used because most of the radiation from the CO_2-laser (wavelength=10.6 μm) was absorbed in the oxides [16]. The molten zone temperature was measured in the infrared radiation region with a custom made infrared pyrometer, while a Thermal Monitor[+] was used to control the laser power. Absolute temperature, however, was not measured because the emissivity of the molten alumina-yittria mixture was not known. All experiments were conducted in air, and neither the crystal nor the source rod was rotated. A TV monitor facilitated the control of seeding and crystal growth. In addition to TV monitors, a Questar 100 long-range optical microscope and a high resolution Kodak Camera were used and linked to a desktop computer via a digitizer.

[#] PRC CORP., Landing, NJ 0785.

2.2 Microstructure and crystallographic characterization

For microstructural analysis the rods, about 2.5 mm in diameter, were sectioned both parallel and perpendicular to the rod axis using a diamond saw. The samples were then polished with diamond-embedded paper down to 0.1μm grit. Since EBSD analysis is very sensitive to surface preparation, samples were ion milled with Ar^+ at 2.0 kV and 5.0 mA for 30 minutes at a 15° incident angle to remove damaged surface layers, thereby improving the quality of the EBSD patterns.

X-ray analysis was performed using a Scintag PTS/Rotating Anode X-ray diffractometer at Oak Ridge National Laboratory. The polished samples were mounted on a goniometer head for precise orientation of the specimen. Several pole figures were taken for various reflections from each phase. Pole figures were used to measure the degree of texture in the crystal and to identify the crystallographic orientation relationships between the phases.

Samples were also examined by SEM and EBSD using a Hitachi™ 3200N variable pressure SEM outfitted with a TexSEM Laboratory™ EBSD camera. Samples were mounted on SEM stubs with conductive carbon tabs and edges were painted with colloidal carbon to reduce charging. A piece of silicon with known orientation was mounted next to each sample for calibration purposes. The SEM was operated at 20 kV and the sample placed at a working distance 19 mm, appropriate parameters for EBSD analysis.

Since the samples are non-conductive, specimen charging occurred in the SEM and obscured the EBSD patterns (Fig. 1a). This charging was minimized by operating the SEM in variable pressure mode at a partial pressure of 5 Pa (Fig. 1b). The resulting patterns were

---

[+] Vanzetti Systems, Stoughten, MA 02072.

automatically indexed by the software once the correct material parameters were input. OIM was performed at several positions along transverse and longitudinal cross-sections of the samples. EBSD patterns were collected from a hexagonal grid with a step size of 0.025 μm, over a total area per scan of 20x50 μm^2. SEM images were acquired with a Robinson-type backscattered electron detector, which is usable under partial pressure conditions and provides compositional contrast.

3. Results and discussion

SEM images of the transverse cross-sections are shown in Figure 2. YAG, having a higher backscattered electron coefficient, appears as the light phase. A "complex regular" microstructure [17], neither fibrous nor lamellar, is evident and consistent with previous observations [11,18,19]. This type of microstructure can occur in eutectics when the major phase, in this case Al_2O_3, has a very high entropy of fusion [2,20]. This results in a faceted growth front of alumina at the solid/ liquid interface and YAG grows cooperatively with the alumina phase. The growth kinetics define the microstructural development and present a large number of orientation relationship for the apparently simple a binary system [21]. Area fractions calculated from SEM images indicate a 53% Al_2O_3 / 47% YAG composition, comparable to that predicted from the eutectic composition of 55% / 45%. Phase domain sizes, as measured by a linear intercept method, varied across the microstructure. The average domain width is largest near the center of the cross-section (~4.1 μm), and becomes systematically smaller towards the edge of the rod, where it is about one-third the size of the central domains. The aspect ratios of the domains in cross section are approximately 1:2, although individual domains are difficult to distinguish since the microstructure is interconnected in three dimensions. Even though the

domain sizes change radially, the morphologies and aspect ratios remain consistent across the sample. The decrease in domain size is due to the fact that the molten zone is heated from the surface, which leads to a radial increase in temperature of the molten zone from the center to the edge. The thermal gradient along the growth direction at the liquid-solid interface is therefore larger near the edges of the sample, resulting in decreased spacing between the alternating phases. The radial temperature gradient and the concomitant microstructural gradient will scale with the diameter of the sample rod.

Even though changes in phase domain sizes were anticipated in the radial direction, they were not expected along the length of the fiber because the heat transfer conditions do not change axially during growth. As shown in Figure 3, however, changes in domain sizes and morphologies do occur along the growth axis. Periodic banding appears, as is found in certain oxide systems [22], consisting of abrupt transitions from larger lamella to smaller lamella. An exact explanation for the development of banding structure is currently lacking. It may, however, be due to the freezing of the boundary layer at the liquid-solid interface ahead of solidification front. The Al_2O_3-YAG eutectic belongs to the group of oxide systems with considerably high viscosities [23] and therefore has slow diffusion rates for the constituents. The pull-rate used in the growth of these rods was around 25 mm/hr which may be too fast for this eutectic system since the diffusion kinetics are slow in the melt. Even though there are discontinuities in the phase domain sizes along the growth axis, OIM shows the nominal crystallographic orientations of the phases are consistent along the length of the sample.

XRD pole figures of alumina and YAG are shown in Fig. 4 and reveal the sample texture and crystallographic orientation relationship between the phases. The pole figures indicate that both phases are nearly single crystalline, although two twin-related variants of Al_2O_3 (designated

A1 and A2) are observed. The poles belonging to each twin variant are grouped with black lines in Fig. 4. Comparison of the Al_2O_3 and YAG pole figures indicates the following nominal crystallographic orientation relationships between the two phases:

$$[\bar{1}11]_Y \,\|\, [\bar{1}100]_{A1} \,\|\, [1\bar{1}00]_{A2}$$
$$(1\bar{1}2)_Y \,\|\, (0001)_{A1} \,\|\, (0001)_{A2}$$

in which the directions also correspond to the fiber axis or growth direction. Note that because alumina is non-centrosymmetric, the $[\bar{1}100]$ and $[1\bar{1}00]$ directions are not crystallographically equivalent. Although this general orientation relationship has been observed in other Al_2O_3-YAG DSEs [19, 21], the growth direction is different. Furthermore, these previous studies did not report the twin-related variants.

The crystal was found to have a mosaic structure as shown in Figure 5, a magnified view of the central portion of the YAG {111} pole figure. The mosaicity is anisotropic with a full-width at half-maximum (FWHM) of 2.4° along $[1\bar{1}2]$ and 1.5° along [110]. The alumina $\{1\bar{1}00\}$ pole figure also displays an anisotropic mosaicity with FWHM of 6.1° and 3.0° along the corresponding [0001] and $[11\bar{2}0]$ directions. Careful comparison of the Al_2O_3 and YAG pole figures also indicates a mistilt between the two growth directions of approximately two degrees along $[1\bar{1}2]_{YAG}$, so the orientation relationships given above are only nominal.

Typical EBSD patterns taken from transverse cross-sections are shown in Figure 6. The left pattern, YAG, shows a growth direction of $[\bar{1}11]$ while the right pattern, alumina, shows a direction of $[\bar{1}100]$ in agreement with the x-ray diffraction data. The mistilt between the growth directions for YAG and Al_2O_3 is approximately 1.8° when measured from EBSD patterns.

Normal to the growth axis, the $(1\bar{1}2)$ and (110) planes of YAG are coincident with the (0001) and $(11\bar{2}0)$ planes of Al_2O_3, in complete agreement with the XRD data. Orientation mapping revealed a systematic radial variation in fiber normal direction, as shown in Figure 7. The direction of mistilt roughly follows the $[1\bar{1}2]$ direction in YAG. The radial variation of the growth direction explains the mosaicity observed in the XRD pole figures.

Orientation image maps, shown in Figure 8, are useful for determining the spatial distribution of the two Al_2O_3 orientational variants and defining interface plane orientations. Figure 8 shows a series of OIM maps from a longitudinal cross section of the sample. In Figure 8a, the orientation of the alumina grains with respect to an in-plane transverse direction are shown, and all are oriented with [0001] parallel to this sample axis. In Figure 8b, the orientation of the alumina grains are plotted with respect to the growth axis and here the twin variants are revealed. Figure 8c and d shows corresponding OIM maps for YAG revealing only $[1\bar{1}2]$ parallel to the transverse sample direction (8c), and $[\bar{1}11]$ parallel to the growth direction (8d).

The images show that the twinning in Al_2O_3 occurs within what appears in the SEM images to be single domains. Growth and deformation twins in alumina are typically of either basal or rhombohedral type [24, 25]. It can be seen in this case that the crystallography of the two variants is consistent with a basal twin, that is a two-fold rotation about the [0001] axis. Typically the habit plane of deformation basal twins is the basal plane, however, it has been shown that growth twins may change habit planes from the (0001) to a $\{1\bar{1}01\}$ or $\{1\bar{1}02\}$ plane in order to accommodate boundary migration [26]. The OIM images indicate that the habit plane is of the $\{1\bar{1}02\}$ type.

4. Conclusions

SEM Electron Backscattered Diffraction (EBSD) and x-ray diffraction (XRD) have been used to quantify the microstructure and crystallography of Al_2O_3-YAG directionally solidified eutectics grown by a laser-heated float zone method. The crystallographic orientation relationships of $[\bar{1}11]_Y \| [\bar{1}100]_{A1} \| [1\bar{1}00]_{A2}$; $(1\bar{1}2)_Y \| (0001)_{A1} \| (0001)_{A2}$ were determined. The observation of two twin-related Al_2O_3 variants and their spatial distribution within the sample, allow greater insight into the growth and final crystallographic character of the LFHZ rods. Systematic variations in microstructure in terms of both phase domain size and orientation were observed along the radial direction of the rods as well as along the rod axis. Such detailed quantitative data on the morphology and the crystallography will allow greater accuracy in modeling stresses and deformation in these highly-textured composites.

Acknowledgements

This project was supported by the Department of Energy under grant #DE-FG-02-98ER-45710 and the AFSOR under grant #F49620-99-1-0266. The authors would also like to thank Drs. Thomas Watkins and Camden Hubbard at the Oak Ridge National Laboratory Diffraction Users' Center for their assistance with the x-ray diffraction work performed under the auspices of the ORNL High Temperature Materials Laboratory User Program (U.S. DOE contract #DE-AC05-00OR22752).

References:

1. L.M. Hogan, R.W. Kraft and F.D. Lemkey, Eutectic Grains, in Advances in Materials Research, H. Herman, Editor, Wiley Intersci., New York, 1971, p. 83.
2. V.S. Stubican and R.C. Bradt, Ann. Rev. Mater. Sci. 11 (1981) 267.
3. V.M. Orera, R.I. Merino, J.A. Pardo, A. Larrea, J.I. Peña, C. González, P. Poza, J.Y. Pastor and J. Llorca, Acta. Mater. 48 (2000) 4683.
4. R. Elliot, International Metals Reviews 22 (1977) 161.
5. D.J.S. Cooksey, D. Munson, M.P. Willkinson and A. Hellawell, Phil. Mag. 10 (1964) 745.
6. R.L. Ashbrook, J. Am. Ceram. Soc. 60 (1977) 428.
7. J.W. Moore and L.H. Van Vlack, J. Am. Ceram. Soc. 51 (1968) 428.
8. T. Mah, T.A. Parthasarathy and L.E. Matson, Ceram. Eng. Sci. Proc. 11 (1990) 1617.
9. T.A. Parthasarathy and T. Mah, Ceram. Eng. Sci. Proc. 11 (1990) 1628.
10. T.A. Parthasarathy, T.-I. Mah and L.E. Matson, J. Am. Ceram. Soc. 76 (1993) 29.
11. Y. Waku, N. Nakagawa, T. Wakamoto, H. Ohtsubo, K. Shimizu and Y. Kohtoku, J. Mater. Sci. 33 (1998) 1217.
12. A. Yoshikawa, K. Hasegawa, J.H. Lee, S.D. Durbin, B.M. Epelbaum, D.H. Yoon, T. Fukuda and Y. Waku, J. Crystal Growth 218 (2000) 67.
13. Y. Waku, N. Nakagawa, T. Wakamoto, H. Ohtsubo, K. Shimizu and Y. Kohtoku, J. Mater. Sci. 33 (1998) 4943.
14. L.E. Matson and N. Hecht, J. Europ. Ceram. Soc. 19 (1999) 2487.
15. A. Sayir and S.C. Farmer, Acta. Mater. 48 (2000) 4691.
16. W.W. Duley, Laser Processing and Analysis of Materials, Editor, Plenum Press New York 1983.
17. J.D. Hunt and K.A. Jackson, Trans. AIME 236 (1966) 843.
18. A. Sayir and L.E. Matson. *Growth and Characterization of Directionally Solidified $Al_2O_3/Y_3Al_5O_{12}$ (YAG) Eutectic Fibers.* in *Proceedings of the 4th Annual HITEMP Review.* 1991. Cleveland, OH: NASA Conference Publication.
19. R.S. Hay and L.E. Matson, Acta Metall. Mater. 39 (1991) 1981.
20. J.D. Hunt and D.T.J. Hurle, Trans. AIME 242 (1968) 1043.
21. S.C. Farmer and A. Sayir, Acta. Mater. (2001)
22. S.C. Farmer, A. Sayir and P.O. Dickerson. *Mechanical and Microstructural Characterization of Directionally-Solidified Alumina-Zirconia Eutectic Fibers,.* in *Intl. Symp. In-Situ Comp. Sci. Tech.* 1993, TMS, Warrendale, PA.
23. M.C. Badets, C. Bessada, P. Simon, D. Billiard, A. Douy, D. Massiot, J.C. Rifflet, F. Taulelle and J.P. Coutures. *Material Processing and Characterization of Y3Al5O12 and $CaAl_2O_4$ Glasses Obtained under Contactless Conditions.* in *Proc. VIIth Europ. Symp. on Matels. and Fluid Sciences in Microgravity.* 1990. Oxford, UK.
24. A.H. Heuer, Philosophical Magazine 13 (1966) 379.
25. K.P.D. Lagerlöf, A.H. Heuer, J. Castaing, J.P. Riviere and T.E. Mitchell, J. Am. Ceram. Soc. 77 (1994) 385.
26. K.J. Morrissey and C.B. Carter, J. Am. Ceram. Soc. 67 (1984) 292.

Figure 1.

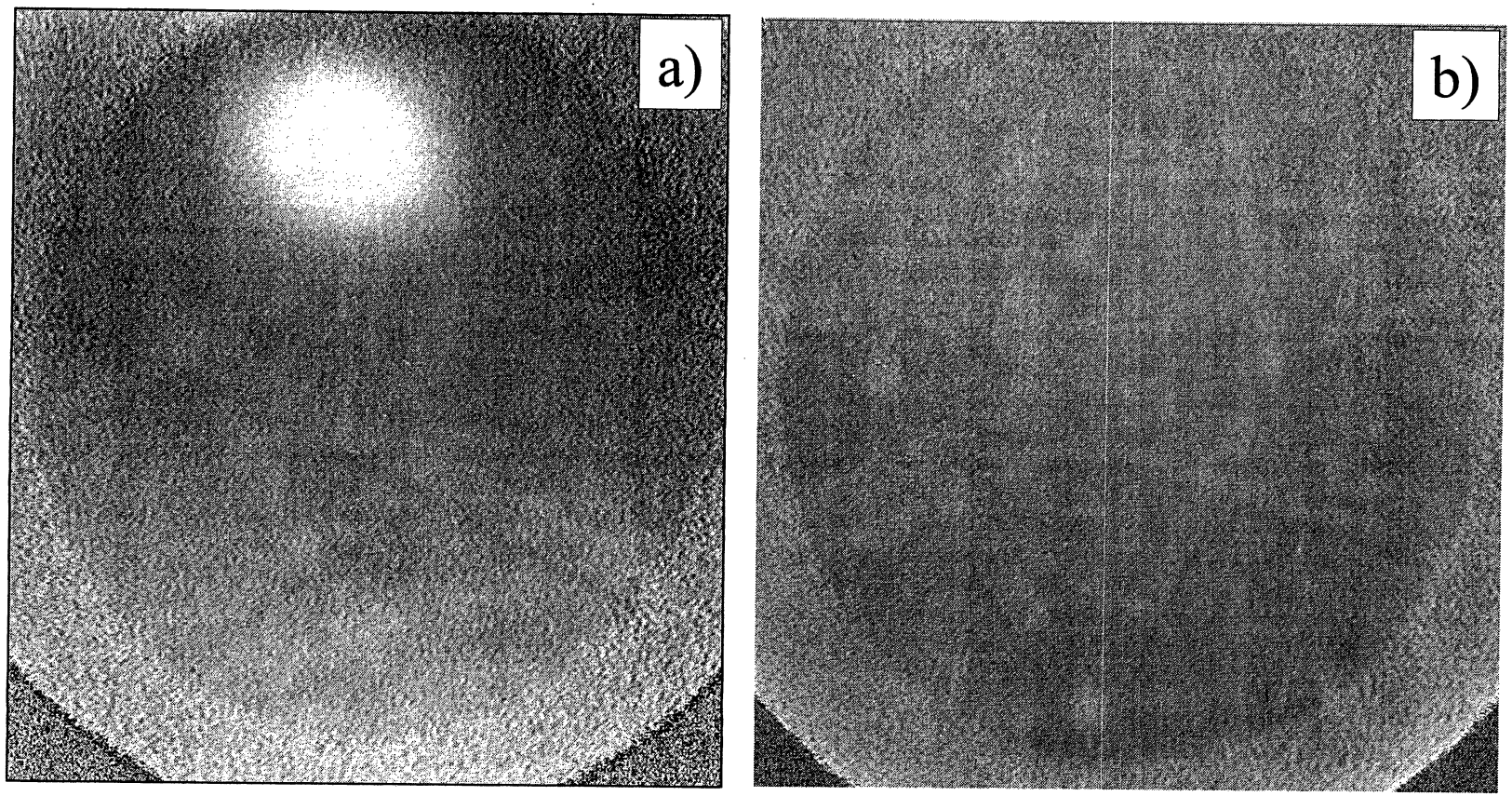

Figure 2.

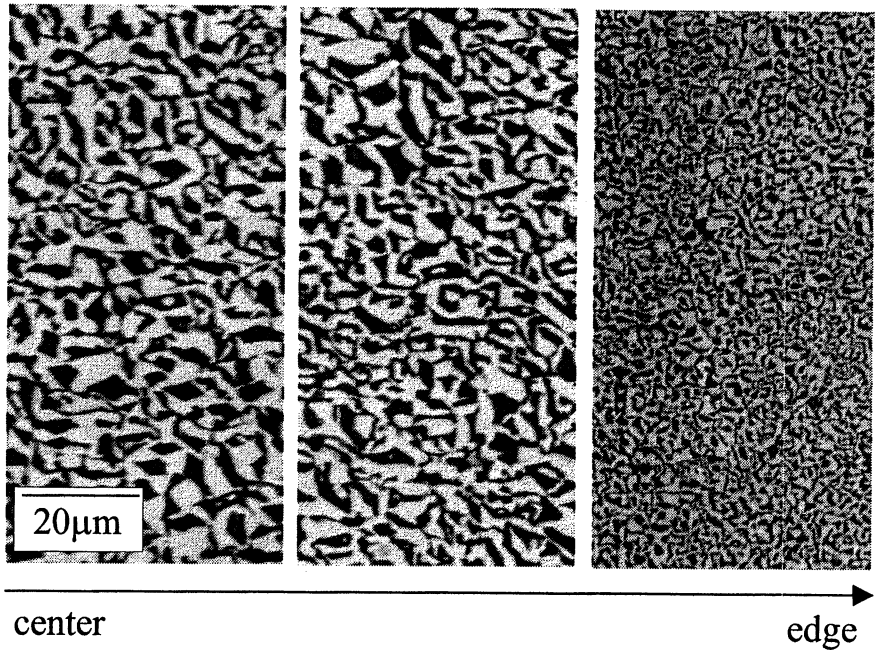

Figure 3.

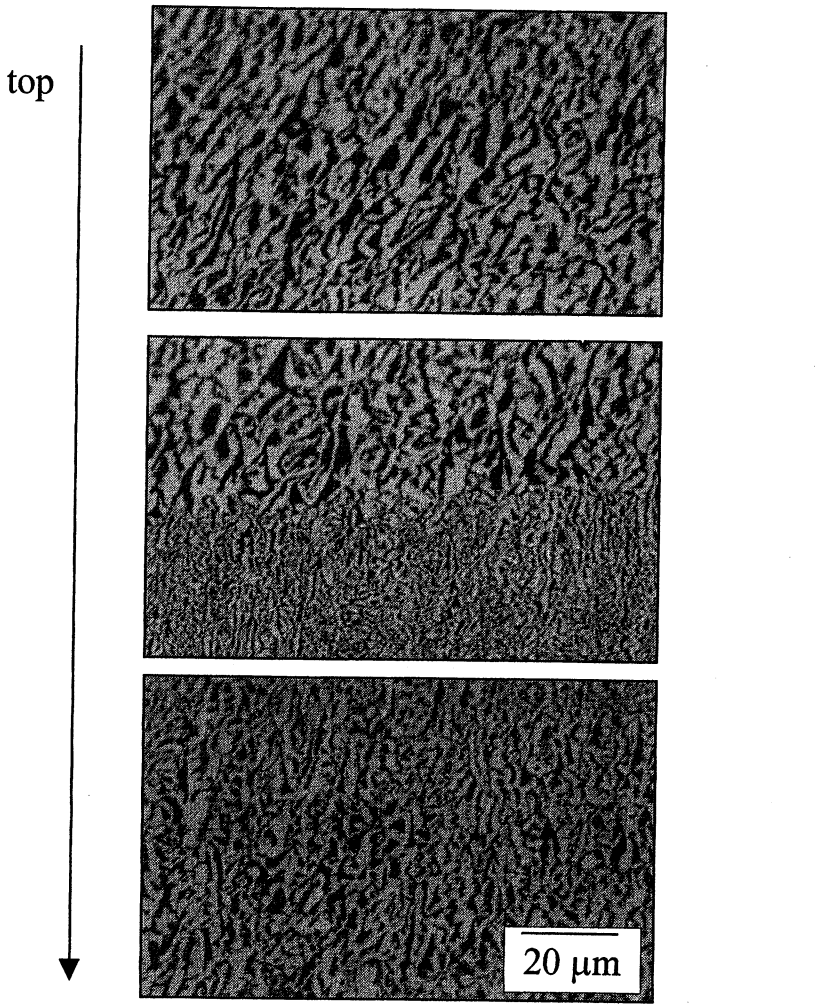
top
20 μm
$[\bar{1}1\,1]_Y \| [\bar{1}100]_{A1} \| [1\bar{1}00]_{A_2}$
$(100)_Y$
$[1\bar{1}2]_Y \| [0001]_{A1} \| [0001]_{A2}$

Figure 4.

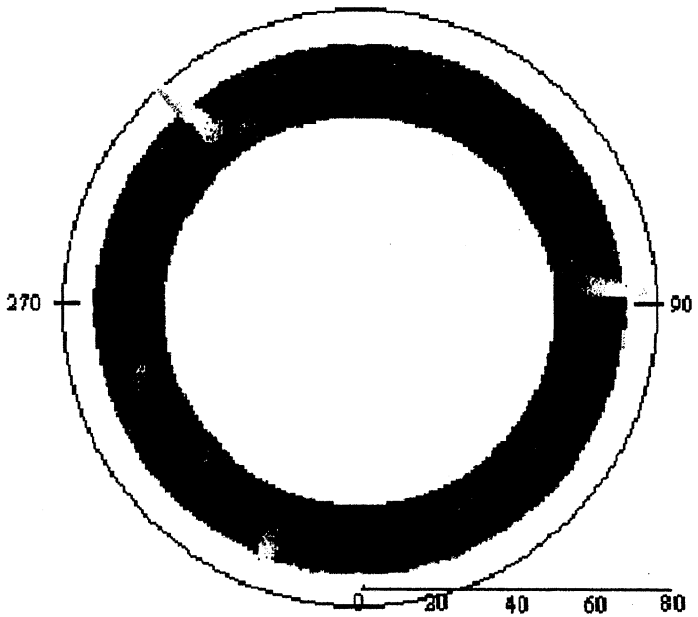

{111}
YAG

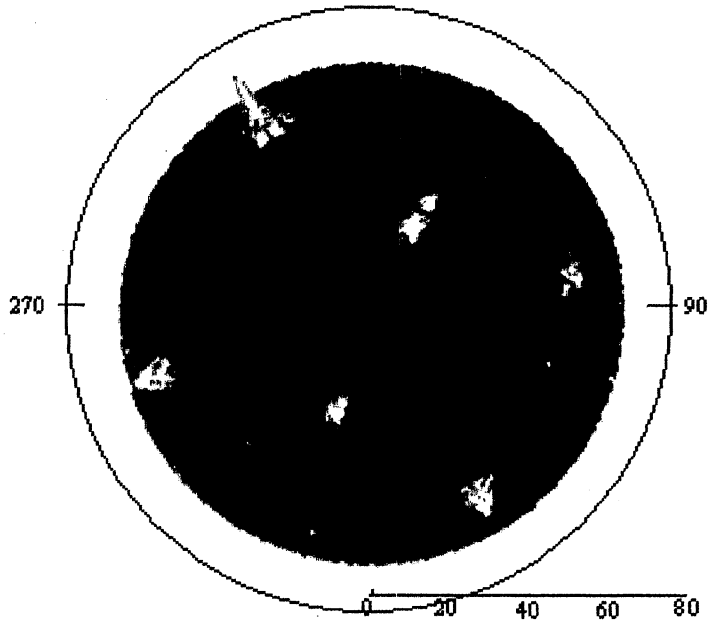

$\{01\bar{1}2\}$
Al_2O_3

Figure 5.

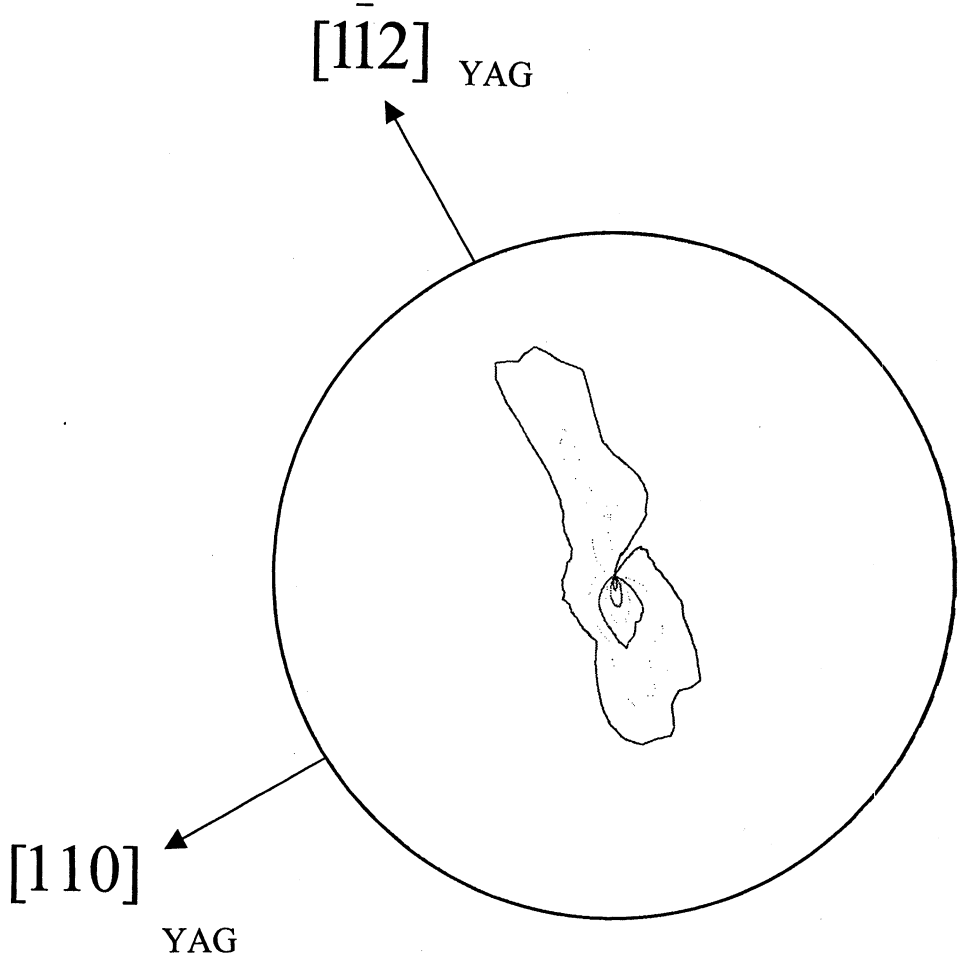

Figure 6.

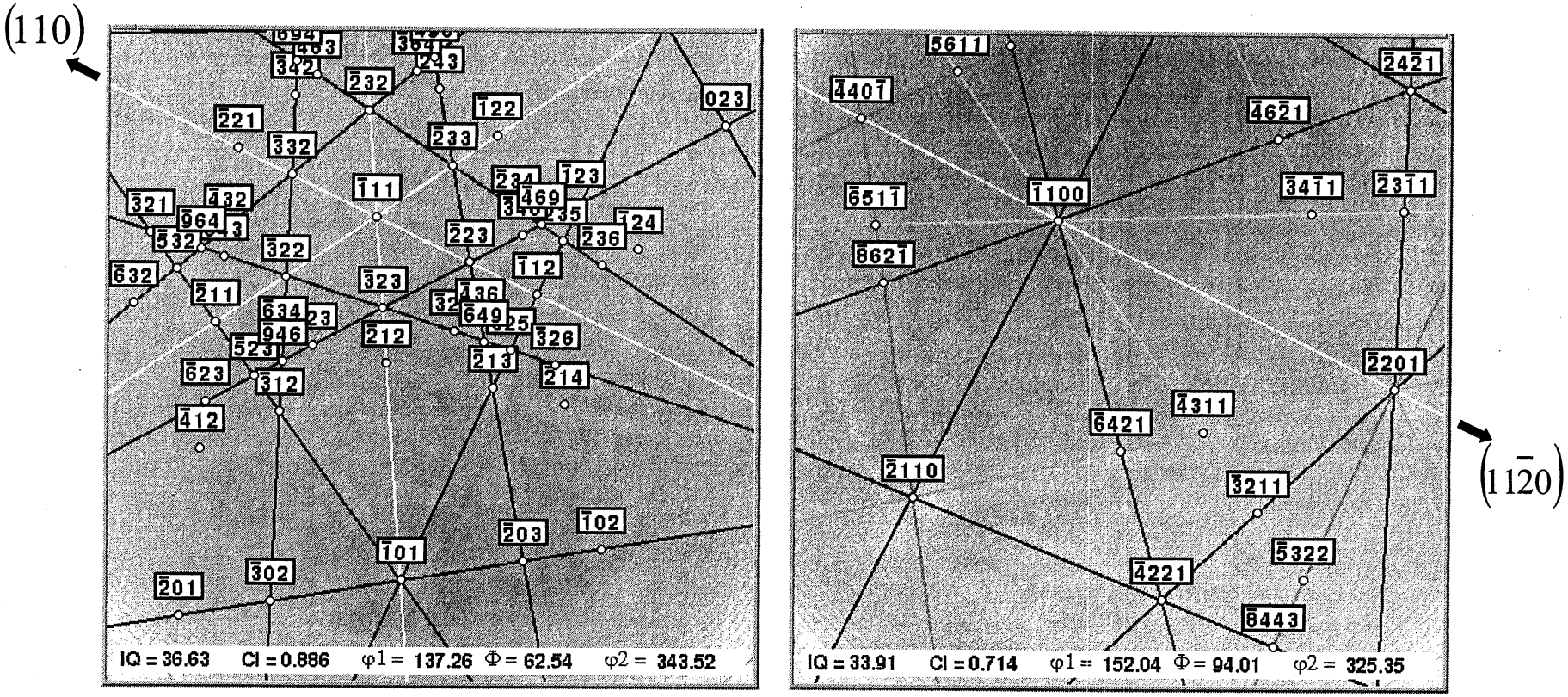

YAG Al_2O_3

Figure 7.

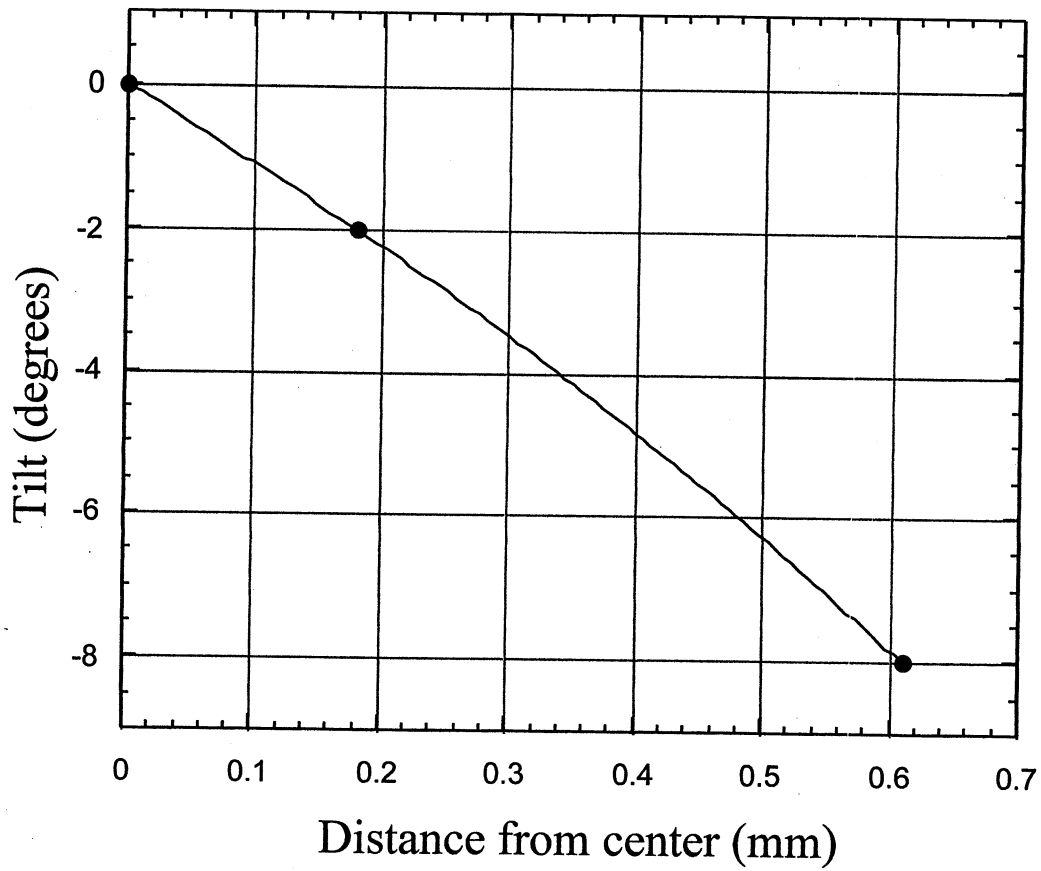
0
-2
-4
-6
-8
Tilt (degrees)
0
0.1
0.2
0.3
0.4
0.5
0.6
0.7
Distance from center (mm)

Figure 8.

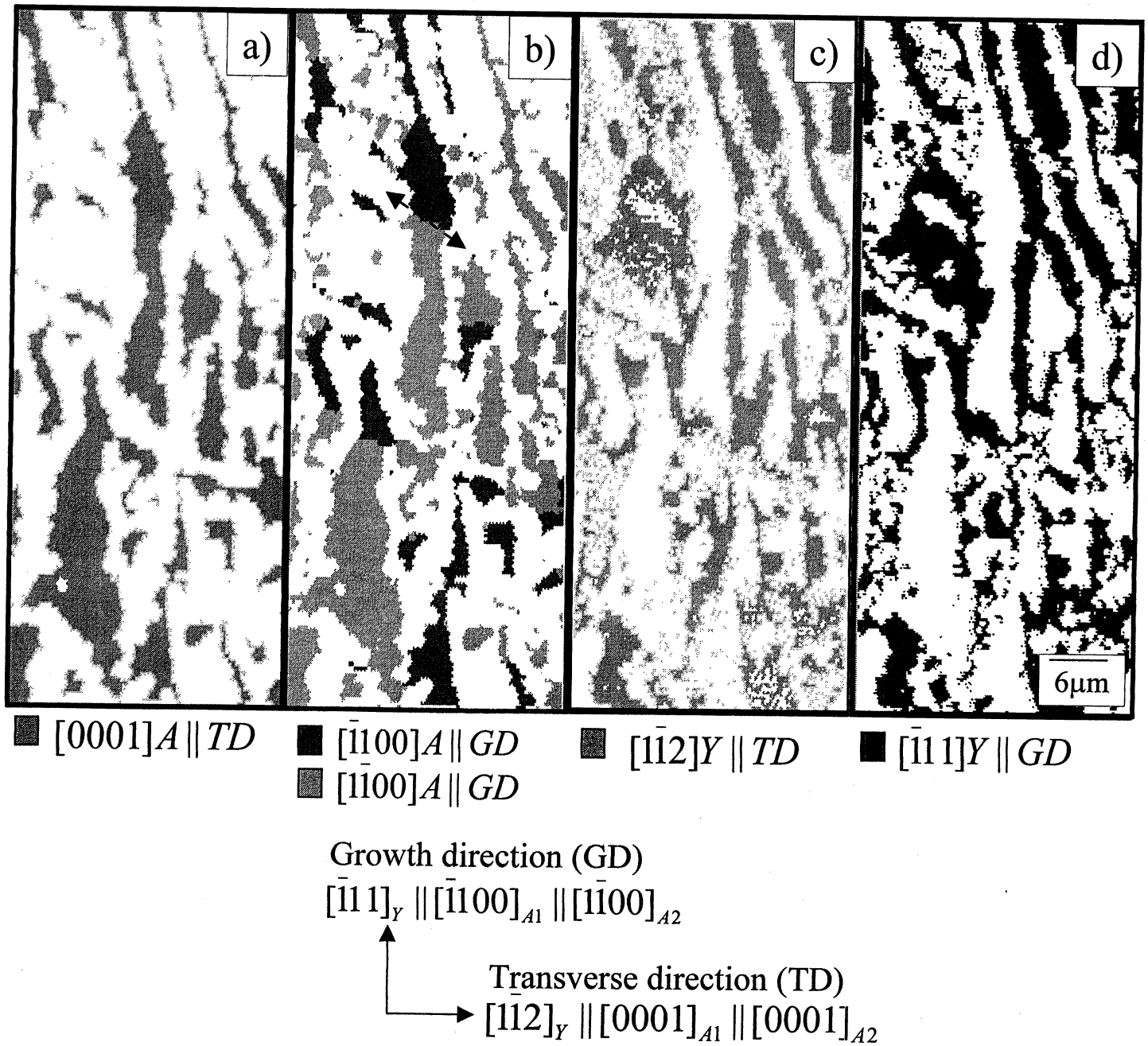
a)
b)
c)
d)
6μm
[0001]A || TD
[$\bar{1}$100]A || GD
[1$\bar{1}$00]A || GD
[1$\bar{1}$2]Y || TD
[$\bar{1}$1 1]Y || GD
Growth direction (GD)
[$\bar{1}$1 1]$_Y$ || [$\bar{1}$100]$_{A1}$ || [1$\bar{1}$00]$_{A2}$
Transverse direction (TD)
[1$\bar{1}$2]$_Y$ || [0001]$_{A1}$ || [0001]$_{A2}$

Figure Captions

Figure 1. EBSD patterns taken a) under high vacuum and b) with 5 Pa pressure of air to reduce charging.

Figure 2. SEM images of an Al_2O_3-YAG DSE transverse cross-section showing radial variation in microstructural scale.

Figure 3. SEM images of microstructural banding along length of an Al_2O_3-YAG DSE rod.

Figure 4. XRD pole figures of a) {111} YAG and b) $\{01\bar{1}2\}$ Al_2O_3. The solid lines in b group the two twin-related variants of Al_2O_3.

Figure 5. Expanded view of central portion of the {111} YAG XRD pole figure plotted from 0-5° shows the anisotropic mosaicity.

Figure 6. EBSD patterns for a) YAG and b) Al_2O_3 from transverse cross-section of rod reveal the crystallographic orientation relationship between the two phases.

Figure 7. Mistilt of growth direction from center to outer radius of an Al_2O_3-YAG DSE as measured by EBSD.

Figure 8. Orientation image maps parallel to the transverse (a and c) and growth (b and d) directions for each phase. The two twin-related variants of Al_2O_3 are revealed in b.